Originally published as:

Strain partitioning and stress rotation at the North Anatolian fault zone from aftershock focal mechanisms of the 1999 Izmit $M_{\mathrm{w}} = 7.4$ earthquake

Marco Bohnhoff, Helmut Grosser and Georg Dresen

GeoForschungsZentrum Potsdam (GFZ), Telegrafenberg, 14473 Potsdam, Germany. E-mail: bohnhoff@gfz-potsdam.de

SUMMARY

We investigate aftershock focal mechanisms of the $M_{\mathrm{w}} = 7.4$ Izmit earthquake of 1999 August 17, on the western North Anatolian fault zone (NAFZ). Spatial clustering and the orientation of 446 fault plane solutions are analysed. The Izmit mainshock occurred as a right-lateral slip on an EW-trending near-vertical fault plane. Aftershock clusters define four individual fault segments. Focal mechanisms surrounding the epicentres of the Izmit and subsequent Düzce mainshock ($M_{\mathrm{w}} = 7.1$, 1999 November 12) indicate predominantly strike-slip but also normal faulting. Aftershocks in the area between the Izmit and Düzce segments are mainly related to EW-oriented normal faulting delineating a small pull-apart structure. Beneath the easternmost Sea of Marmara, alignments of aftershocks suggest branching of the NAFZ into three or more active segments that differ significantly in terms of their focal mechanism characteristics. The distribution of aftershock focal mechanisms corresponds to fault segmentation of the NAFZ in the Izmit-Düzce region produced by coseismic slip. Areas with large amounts of coseismic slip show aftershocks that are predominantly strike-slip, but low-slip barriers show mostly normal faulting aftershocks.

Stress tensor inversions of the aftershock focal mechanisms show rotations of the local stresses following the Izmit mainshock. In the Izmit-Sapanca area, the maximum horizontal compressive stress axis is horizontally rotated counter-clockwise by 8° with respect to the coseismic and long-term regional stress field. Towards the eastern end of the rupture (Karadere-Düzce area), stresses are rotated clockwise. We conclude that the Izmit earthquake caused significant stress partitioning along the rupture. The direction of stress rotation is related to the orientation of the individual fault segments along the NAFZ.

Key words: aftershocks, fault plane solutions, North Anatolian Fault, seismotectonics, stress tensor inversion.

GJI Seismology

1 INTRODUCTION

The Izmit $M_{\mathrm{w}} = 7.4$ (1999 August 17) earthquake occurred on the northern strand of the North Anatolian fault zone (NAFZ) in the Gulf of Izmit region. The rupture extended about 140 km between the Sea of Marmara and the Düzce region along a right-lateral, predominantly EW-trending, near-vertical fault plane (Fig. 1). Estimates of average coseismic fault slip vary between 2.5 m (e.g. Tibi *et al.* 2001) and 2.9 m (Bouchon *et al.* 2002) from inversion of teleseismic data and records of near-fault accelerometers, respectively. Maximum slip at the surface reached about 5–6 m (Barka *et al.* 2002; Bouchon *et al.* 2002; Bos *et al.* 2004, others). The direction of slip corresponds well to the overall horizontal GPS-derived 2–2.5 cm yr^{-1} westward motion of the Anatolian block with respect to Eurasia (e.g. Noomen *et al.* 1996; McClusky *et al.* 2000, Fig. 1a). Analyses of surface rupture, teleseismic, strong motion and

geodetic data all indicate separation of the mainshock into subevents occurring on distinct fault segments (e.g. Reilinger *et al.* 2000; Tibi *et al.* 2001; Barka *et al.* 2002; Delouis *et al.* 2002; Gülen *et al.* 2002; Bos *et al.* 2004). The western termination of the Izmit rupture is located offshore beneath the Sea of Marmara (e.g. Wright *et al.* 2001), possibly extending to the area south of the Prince Islands about 20 km southeast of Istanbul (Bouchon *et al.* 2002; Özalaybey *et al.* 2002). Rupture propagation towards the east ended near Düzce where a large earthquake occurred 87 days after the Izmit event (1999 November 12, $M_{\mathrm{w}} = 7.1$). Nodal planes of focal mechanisms for the Izmit main event, the major subevent (S2, Tibi *et al.* 2001) and for the Düzce earthquake strike dominantly EW (Fig. 1b). The combined rupture length for the Izmit and Düzce earthquakes is estimated to be about 200 km. The Marmara region west of the Izmit rupture is considered to be a seismic gap. Recent estimates of Coulomb stress changes and earthquake probability
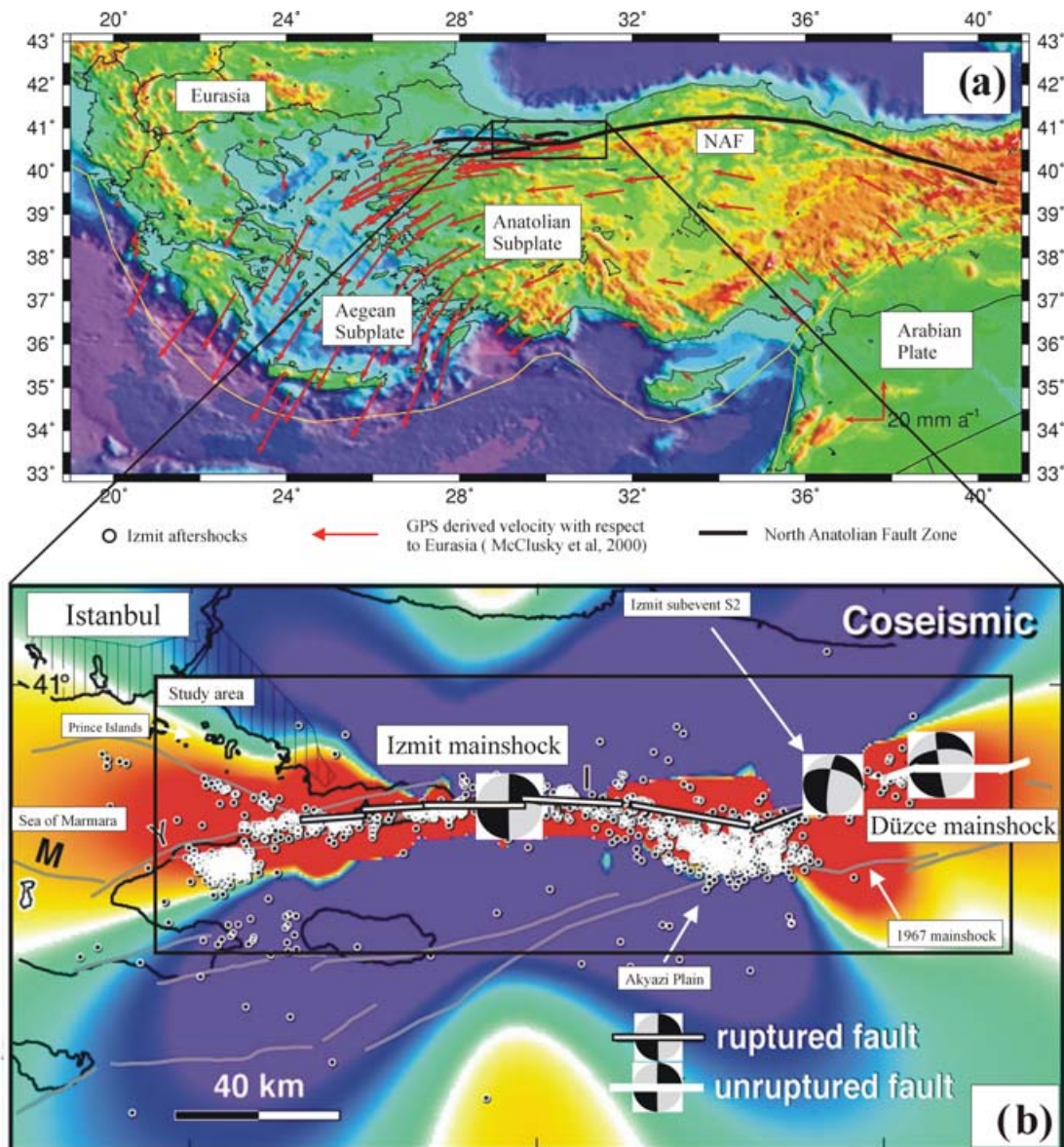
Figure 1. (a) Location map of the Aegean-Anatolian region (courtesy of K. Fischer). Red arrows represent the GPS-derived horizontal velocity field (after McClusky *et al.* 2000). The bold black line is the simplified trace of the North Anatolian fault zone (NAFZ). The Izmit segment of the NAFZ is indicated by the black rectangular and enlarged in Fig. 1(b). (b) Coulomb stress map after the Izmit M_w = 7.4 (1999 August 17) earthquake (after Parsons *et al.* 2000, their Fig. 1). Red and blue colours indicate regions of increased and decreased Coulomb stress, respectively. White dots indicate locations of Izmit aftershocks. Fault mechanisms are shown for the Izmit mainshock, Izmit subevent S2 (M_w = 6.9, Tibi *et al.* 2001) and Düzce mainshock (M_w = 7.1, 1999 November 12) from West to East. The black rectangle indicates the area investigated in this study.

calculations (Parsons *et al.* 2000; Wright *et al.* 2001; Parsons 2004) suggest that the Izmit earthquake increased the seismic hazard for the Marmara and Düzce regions (Fig. 1b). The Düzce earthquake as also the 1992 Erzincan event indicate an eastward propagation of mainshocks. However, this is in contrast to an overall westward migration of strong earthquakes along the NAFZ observed since the 1939 Erzincan event (e.g. Töksöz *et al.* 1979; Stein *et al.* 1997).

Here, we focus on aftershocks of the Izmit earthquake covering the time span 1999 August 17–November 12. We analyse the spatiotemporal evolution of aftershock focal mechanisms and perform stress tensor inversion to determine the local stress field. The results are compared to the coseismic rupture and afterslip of the Izmit earthquake and to the regional tectonic setting.

2 ANALYSIS OF AFTERSHOCK FOCAL MECHANISMS

The data set consists of 446 aftershock focal mechanisms out of which 254 were determined from recordings of a 41-station seismic network covering the entire Izmit rupture area. A part of the network (29 stations) was installed four days after the Izmit mainshock and was operated by the German Task Force for earthquakes hosted at the GeoForschungsZentrum Potsdam (Grosser *et al.* 1998; Baumbach *et al.* 2003). These stations enlarged a 12-station network that had been installed in that region in 1996 (SABONET, Milkereit *et al.* 2000). Fault mechanisms for these 254 events were determined by a grid search over all possible fault plane solutions assuming a double-couple model (FPFIT program, Reasenberg & Oppenheimer 1985).
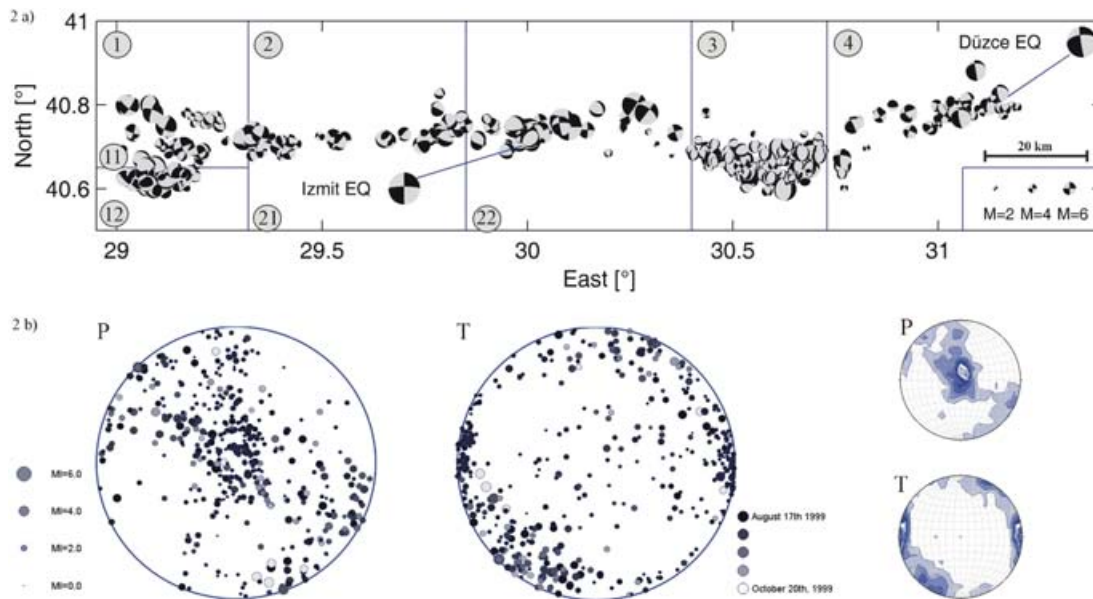
Figure 2. (a) Epicentre distribution of the 446 fault plane solutions analysed in this study in map view of the lower hemisphere. The size of the beachballs scales with magnitude. The Izmit and Düzce mainshocks are indicated by their fault mechanisms. Numbers indicate (sub) segments along the Izmit rupture zone that were identified based on spatial clustering of fault mechanisms as discussed in the text. (b) Distribution of P and T axes for the 446 fault plane solutions in polar projection of the lower hemisphere. The size of circles scales with magnitude and the shading indicates the hypocentral time (lighter colour $\approx$ later occurrence). In addition we plotted the density distribution for the P and T axes of the entire data set where shading is scaled to maximum for P and T separately.

Almost complete spatial coverage allowed us to reject all events for which the grid-search results suggested multiple fault plane solutions. The accuracy of individual fault mechanisms is 5° for strike, dip and rake.

In addition, 192 fault plane solutions were collected from published studies. The data are from seismic networks with different geometries covering parts of the Izmit rupture area (Karabulut *et al.* 2002; Özalaybey *et al.* 2002; Polat *et al.* 2002). We also include source mechanisms determined by regional moment tensor inversion of the 30 largest Izmit aftershocks (Örgülü and Aktar, 2001). Multiple occurrences of events are excluded from the data set. We estimate the average orientation error of the fault plane solutions in our data set to be ∼10°. The events cover an area between 28.95°–31.4°E and 40.5°–41.0°N and extend to a maximum depth of 18 km (a single event was located at a depth of 23 km, Fig. 2a).

Spatial clustering of the aftershock locations, fault mechanisms and slip directions are investigated statistically. Temporal distribution and event magnitude are also considered. Orientation distribution of aftershock fault mechanisms is given by the respective P and T axes in lower-hemisphere polar projection plots (Fig. 2b). P and T axes represent the centre of the dilatational and compressional quadrants of the focal mechanisms, indicating the direction of maximum compressional and dilatational deformation, respectively.

3 SEGMENTATION OF THE IZMIT RUPTURE ZONE

Aftershock epicentres are clustered in an E-W direction along the NAFZ between 40.55°N and 40.90°N. The distribution of P and T axes suggests a spatial separation of the 446 fault mechanisms into four major segments along the rupture zone (Fig. 2a). Between 29.5°E and 30.4°E, aftershock epicentres follow the strike of the

rupture trace of the Izmit event. A prominent cluster containing 169 events is located at about 30.6°E in the Akyazi area. Trains of aftershocks indicate activation of secondary fault structures inclined by ∼10° to the E–W trending NAFZ. In general, P axes are either subvertical or subhorizontal trending at N90°E–N180°E; T axes are predominantly subhorizontal with a large scatter (N160°E–N290°E). The distribution of P and T axes indicates that strike-slip and normal faulting dominate the Izmit rupture after the mainshock.

Segment 1 (28.95°E–29.30°E) contains 110 fault plane solutions covering the western termination of the Izmit rupture located beneath the easternmost Sea of Marmara (Fig. 3). Aftershock clusters indicate activation of three different branches of the NAFZ. For each branch, the fault mechanisms are very similar and one of the two nodal planes often coincides with a mapped fault. The northern part (subsegment 11) contains mainly strike-slip events located on a ∼N305°E-striking vertical plane. A series of events indicating normal faulting is aligned along a parallel small fault segment (Fig. 3). The southern branch (subsegment 12) contains NNE–SSW-extensional normal fault events and some NW–SW-compressional thrust fault events revealing a complex local fault structure. This area largely coincides with the Yalova cluster that showed swarm activity covering a time period of several years prior to the Izmit event (e.g. Gurbuz *et al.* 2000; Baris *et al.* 2002).

Segment 2 (29.3°E–30.4°E) covers the Izmit-Sapanca area and contains 107 aftershocks and the Izmit mainshock epicentre (Fig. 4). In the western part (subsegment 21), aftershock epicentres are aligned with the surface rupture trace trending E–W. P and T axes indicate a wide distribution of focal mechanisms. However, in the eastern part (subsegment 22) the aftershock locations trend ∼N80°E and, therefore, strike at an angle of ∼10° to the rupture trace and slip direction of the Izmit mainshock. Focal mechanisms indicate predominantly right-lateral strike-slip and some normal faulting.
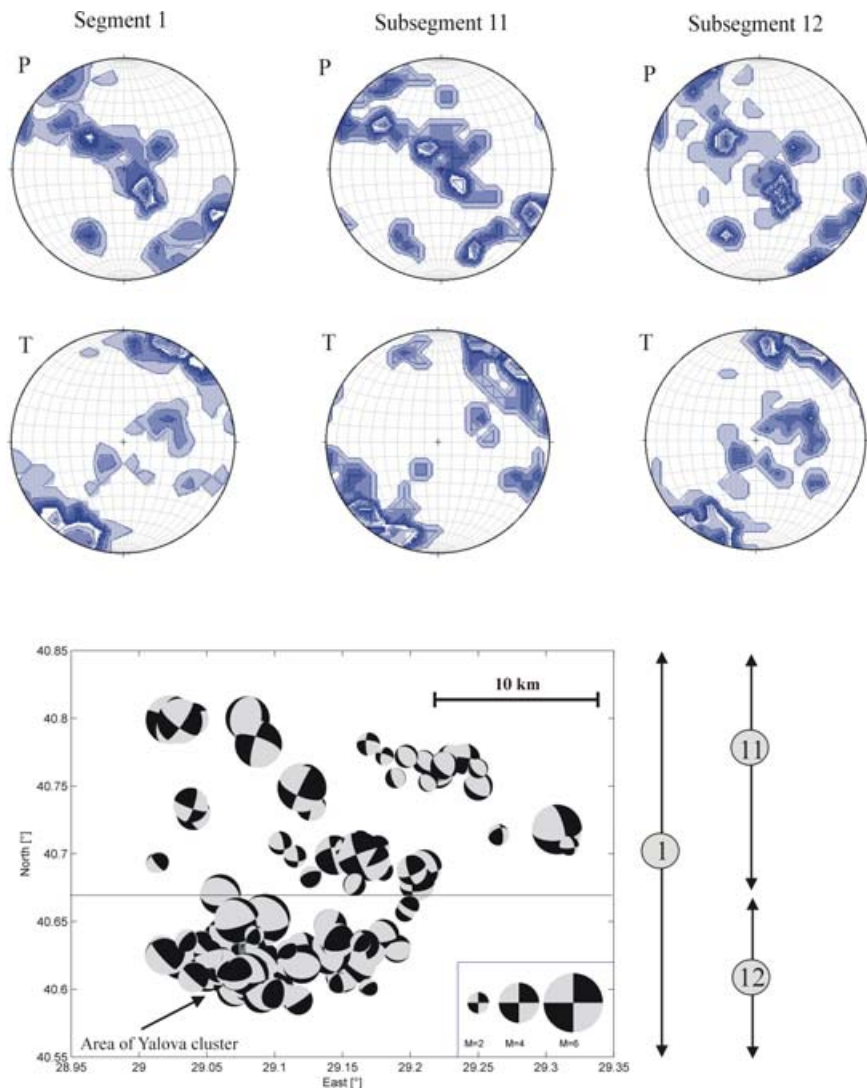
Figure 3. Density distribution of *P* and *T* axes and map view of fault plane solutions for all events contained in segment 1 (see Fig. 2). The epicentral distribution exhibits trains with highly similar focal mechanisms matching one of the two possible fault planes. This suggests further subdivision into a northern (11) and a southern (12) subsegment (see text for details).

P axis trends and the nodal planes of individual strike-slip events are rotated counter-clockwise by ~10° with respect to the Izmit main shock focal mechanism.

Segment 3 (30.4°E–30.85°E) is located near the town of Akyazi at a triple junction formed by the Izmit-Sapanca and Karadere-Düzce faults and the ESE-striking Mudurnu fault, where a major earthquake occurred in 1967 (Fig. 1b). This segment contains 169 fault plane solutions, that is, 40 per cent of the entire data set. The focal mechanisms of a dense cluster of events indicate E–W extensional normal faulting (Fig. 5). The high aftershock activity is in striking contrast to the small coseismic displacement of <1 m in this area suggested by surface slip and the inversion of strong motion data (Barka *et al.* 2002; Bouchon *et al.* 2002; Langridge *et al.* 2002). The ESE-striking southern branch of the NAFZ exhibited few aftershocks and no surface slip, possibly due to stress relaxation after the 1967 event.

Segment 4 (30.85°E–31.3°E) contains 60 aftershock fault plane solutions, including the epicentres of the Izmit subevent S2 (Tibi *et al.* 2001) and the Düzce mainshock (Fig. 1b). Aftershock locations

indicate a 25° clockwise rotation with respect to the local trend of the Karadere segment (N65°E). *P* axes of the events are in accordance with activation of an ENE–WSW striking fault segment. In general, a broad distribution of focal mechanism parameters reflects uniform right-lateral strike-slip with frequently E–W-oriented sets of nodal planes (Fig. 6).

4 STRESS TENSOR INVERSION

The aftershock fault mechanisms investigated in this study were used for an inversion of the stress tensor. Stress tensor inversion techniques using focal mechanisms have been discussed in detail by various authors (e.g. Gephart & Forsyth 1984; Gephart 1990; Michael 1987a, 1991; Hardebeck & Hauksson 2001; Bohnhoff *et al.* 2004). We use a technique proposed by Michael (1984, 1987a). The analysis allows us to estimate the orientation of the three principal stresses (σ_1 = maximum compressive stress, σ_2 = intermediate and σ_3 = minimum) and the stress ratio $R = (\sigma_2 - \sigma_3)/(\sigma_1 - \sigma_3)$,
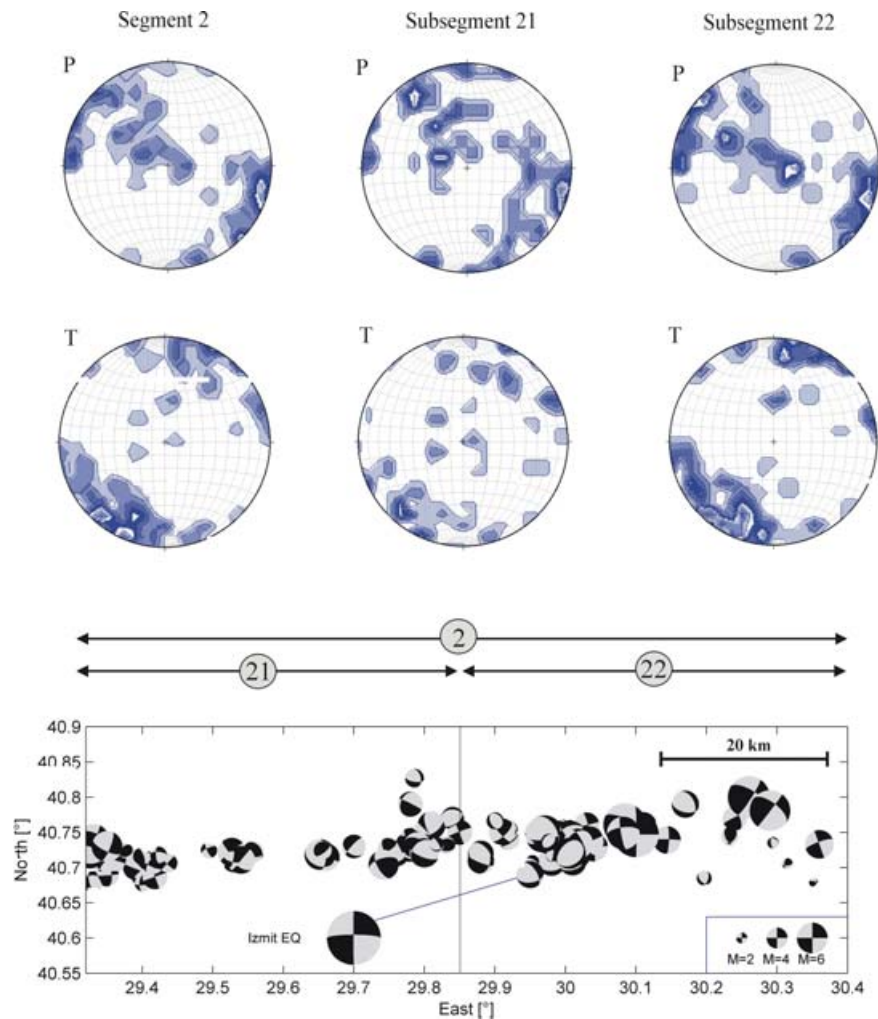
Figure 4. Density distribution of *P* and *T* axes and map view of fault plane solutions for all events contained in segment 2 that includes the epicentre of the Izmit mainshock. Scanning the data from West to East allows identifying a significant variation in clustering of similar mechanisms within this segment. The eastern subsegment (22) consists dominantly of strike-slip mechanisms in good accordance with the mainshock in first order approximation and contains a number of NNE–SSW extensional normal faulting events; the western subsegment (21) does not exhibit a preferred fault mechanism. In subsegment 22, hypocentres follow a trend that is inclined to the E–W striking fault west of the Izmit epicentre; *P* axis distribution in this subsegment shows several preferred orientations some of which are rotated by ∼10° with respect to the Izmit mainshock.

$0 \leq R \leq 1$ (with $R < 0.5$ and $R > 0.5$ indicating a transpressional and transtensional regime, respectively). The method is based on the assumptions that

(1) in the area of investigation stresses remain uniform in time and space,
(2) earthquakes represent shear dislocations on existing faults, and
(3) slip occurs in the direction of the maximum resolved shear stress on the fault plane.

Heterogeneity of the stress field is reflected by the misfit level and the width of the confidence interval of the inversion (Table 1 and Fig. 7). For each stress inversion, 2000 bootstrap iterations were performed.

The stress inversion of all focal mechanisms results in a normal-faulting regime with clear separation of the principal stresses (Fig. 7). The maximum compressive stress σ_1 is almost vertical and σ_3 is horizontal, trending N237°E. This result is in contrast to estimates of the regional long-term stress field in NW Turkey

that suggest predominantly strike-slip deformation with a ∼N125°E striking subhorizontal direction of σ_1 (Kiratzi 2002; Heidbach *et al.* 2004; Reinecker *et al.* 2004, see Table 1) and points towards significant variations of stress field orientation along the NAFZ after the Izmit event. Furthermore, the data set as a whole is dominated by the large number of events located in segment 3 showing predominantly normal faulting. To investigate further local variations in the stress regime along the Izmit rupture we subdivided the catalogue according to the segmentation identified from the distribution of *P* and *T* axes (segments 1–4). Stress inversion of the four segments reveals a clear variation of the local stress field orientation along the Izmit rupture (Fig. 7). For the Akyazi area (segment 3), the results indicate a separation of the principal stresses (black dots) with narrow 1σ (68 per cent, dark grey) and 2σ (95 per cent, light grey) confidence intervals. For the remaining segments, however, confidence intervals for the largest and intermediate principal stresses form a girdle (Fig. 7).

Stress ratio ($R = 0.83$) and confidence intervals for segments 1 and 2 reflect the dominating deformation regimes (strike-slip
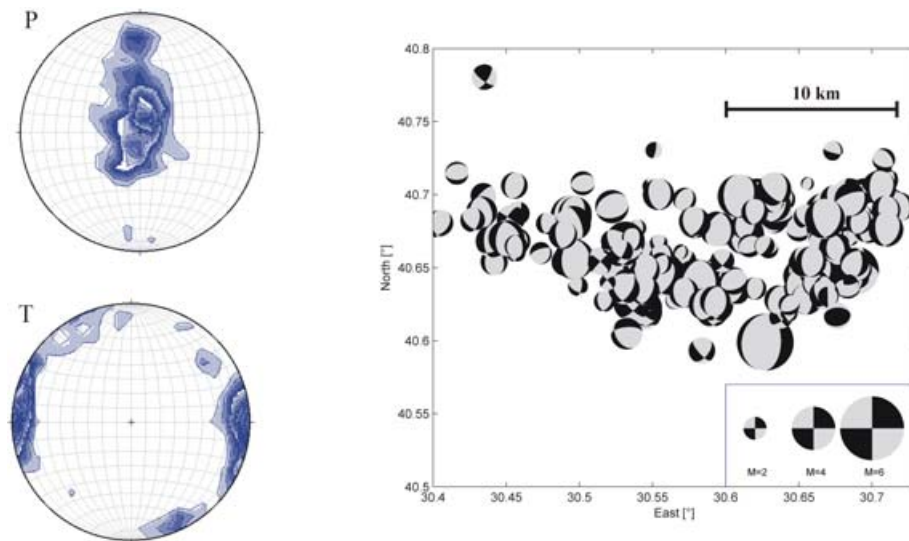
Figure 5. Density distribution of *P* and *T* axes and map view of fault plane solutions for all events contained in segment 3. A dominant EW-extensional normal faulting regime is observed along this segment that contains about 40 per cent of the entire set of fault plane solutions analysed in this study. Different to the three other segments no alignment is observed from the distribution of aftershock hypocentres; instead the aftershock activity cover the entire Akyazi plain that is identified as a pull-apart structure.
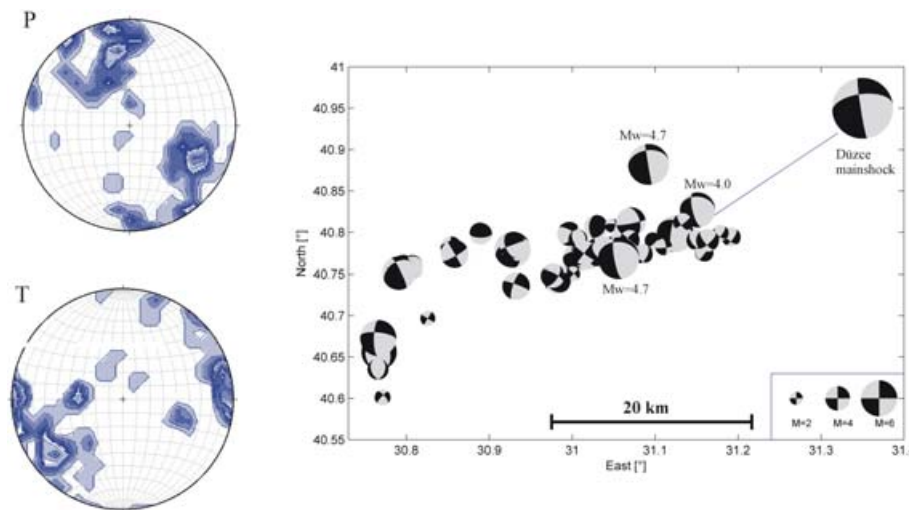

Figure 6. Density distribution of *P* and *T* axes and map view of fault plane solutions for all events contained in segment 4 that includes the Karadere segment and the Düzce mainshock epicentral area. A dominant strike-slip mechanism is observed for this easternmost part of the Izmit rupture area. Events with annotated magnitude mark the largest and earliest aftershocks in this segment and are discussed in the text. Most hypocentres are aligned on an almost EW-trending direction that is inclined to the local fault trend of N65°E (Karadere segment, see Fig. 8) by ∼25°.

and normal faulting). The principal stresses σ_1 and σ_2 differ only slightly in their magnitude and both stress directions trend roughly NW–SE within both segments (N314°E and N117°E, respectively). The minimum compressional stress σ_3 is clearly differentiated from σ_1 and σ_2, trending subhorizontally NE–SW. The Izmit-Sapanca area (segment 2) includes the Izmit mainshock epicentre. Here, the post-seismic trend of σ_1 indicates a counter-clockwise rotation of 8° with respect to the regional stress field and the coseismic stress field derived from inverting the focal mechanisms of the six Izmit subevents (Gülen *et al.* 2002, Table 1). In the Akyazi area (segment 3), directions of principle stresses $\sigma_1 - \sigma_3$ are well constrained and correspond to an E–W extensional normal faulting regime. The relative stress magnitude $R = 0.62$ indicates that the magnitude of σ_2 is close to the mean of σ_1 and σ_3.

The easternmost segment 4 covers the N65°E-trending Karadere segment pointing towards the Düzce area where a $M_w = 7.1$ earthquake occurred 87 days after the Izmit mainshock. Stress orientation and confidence intervals for this area indicate a strike-slip regime with a stress ratio of $R = 0.63$ (Fig. 7). The maximum principle stress (σ_1) is subhorizontal and trends N159°E, indicating a clockwise rotation with respect to the regional stress field of > 30°.

5 DISCUSSION

5.1 Segmentation of the Izmit rupture zone

The Izmit earthquake ruptured a 140 km-long E–W trending segment of the western NAFZ. Offshore in the easternmost Sea of

Table 1. Overview on stress field orientations along the Izmit part of the NAFZ observed from the different sources and determined in this study. Data sets cover different areas and time intervals. Azimuth (tr = trend) and angle of incidence (pl = plunge) for the principal stresses are given in N over E and against horizontal, respectively.

Area covered	Time covered	Focal mech. [no.]	σ_1 (tr/pl) [°]	Std [°]	σ_2 (tr/pl) [°]	Std [°]	σ_3 (tr/pl) [°]	std [°]	Misfit	R	Source
NW Turkey	1943–1999	11	126/3	13	269/86	–	35/3	13	3.3°[c]	0.5	Kiratzi (2002)
NW Turkey	1943–1999	13[b]	124/-[a]	(25)	–/90	–	34/–	–	–	–	Reinecker *et al.* (2004) Heidbach *et al.* (2004)
E Sea of Marmara	1996 Jan–Sep	37	305/1	14	206/86	20	35/4	17	0.31	0.5	Ergin *et al.* (1997)
Izmit rupture	Coseismic Izmit	6	124/3	15	231/79	15	34/11	15	0.31	0.5	Gülen *et al.* (2002)
Izmit rupture	Post-seismic Izmit	30	316/13	10	81/68	10	222/18	10	0.16	0.74	Örgülü & Aktar (2001)
Izmit rupture (segment 0)	Post-seismic Izmit	446	66/87	6	327/0	6	237/3	6	0.22	0.64	This study
E Sea of Marmara (segment 1)	Post-seismic Izmit	110	314/23	6	144/57	6	45/ 4	6	0.20	0.83	This study
Izmit Sapanca (segment 2)	Post-seismic Izmit	107	117/15	6	347/67	6	212/17	6	0.22	0.83	This study
Akyazi plain (segment 3)	Post-seismic Izmit	169	190/74	6	3/15	6	94/1	6	0.09	0.62	This study
Karadere Düzce (segment 4)	Post-seismic Izmit	60	339/6	8	49/74	8	251/15	8	0.19	0.63	This study

standard deviation (std) refers to the trend for σ_{1-3}.
[a]S_H.
[b]and shallow boreholes.
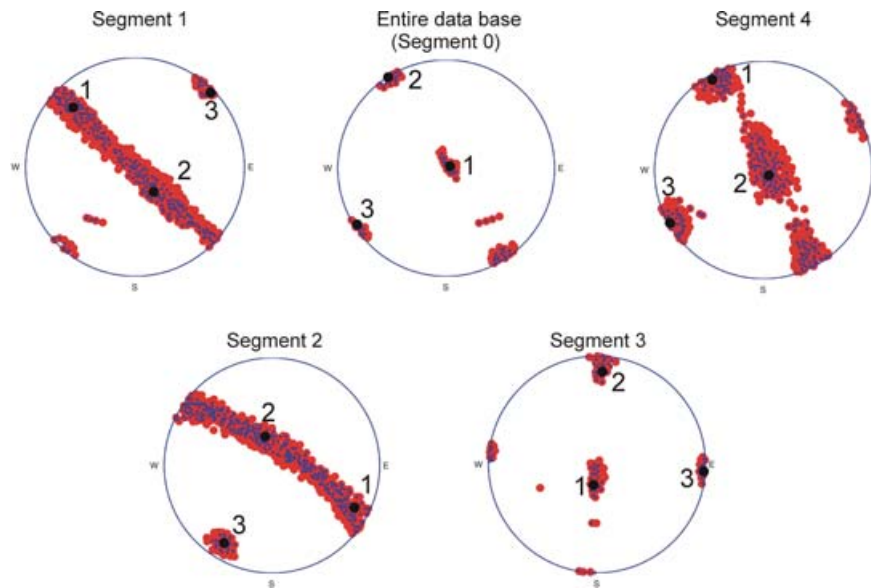[c]misfit as given by the FMSI routine (Gephart & Forsyth 1984).

Figure 7. Results of stress tensor inversion for the entire data base containing 446 fault plane solutions and the four segments (see Figs 3–6 for map view of fault mechanisms contained therein). Bold black dots represent the best fitting orientations for the three principal stresses (σ_1 = maximum compressional stress, σ_2 = intermediate; σ_3 = minimum). Small and large dots represent the 1σ (68 per cent) and 2σ (95 per cent) confidence intervals, respectively.

Marmara, the NAFZ splays into different branches producing a complex network comprising the Izmit-Sapanca, Düzce, Iznik, Geyve and Mudurnu faults (Fig. 8). The width of this network is about 30 km and thus on the order of the thickness of the seismogenic upper crust. Regional tectonics in western Turkey are dominated by right-lateral strike-slip along the ~EW-trending NAFZ and a NE–SW extensional regime associated with a >3 cm yr^{-1} SSW-ward migration of the South Aegean domain with respect to stable Eurasia (e.g. McClusky *et al.* 2000; Flerit *et al.* 2004). At the NAFZ, GPS data indicates westward motion of northwestern Anatolia at about 2–2.5 cm yr^{-1}. In this tectonic regime, the Sea of Marmara

formed as a large pull-apart structure (e.g. Armijo *et al.* 1999) in a transtensional environment. On a smaller scale, fault segments are separated by releasing bends and small-scale pull-apart structures such as Izmit Bay and Lake Sapanca.

Analysis of aftershock focal mechanisms along the Izmit rupture reveals predominantly strike-slip and normal faulting events in combination with few thrust events, indicating that strain partitioning and variations in the local stress field is a dominant feature within this region. Thrust faulting is restricted to a small area near Yalova where pronounced seismicity was observed prior to the Izmit mainshock (Gurbuz *et al.* 2000; Baris *et al.* 2002). In the Izmit-Sapanca
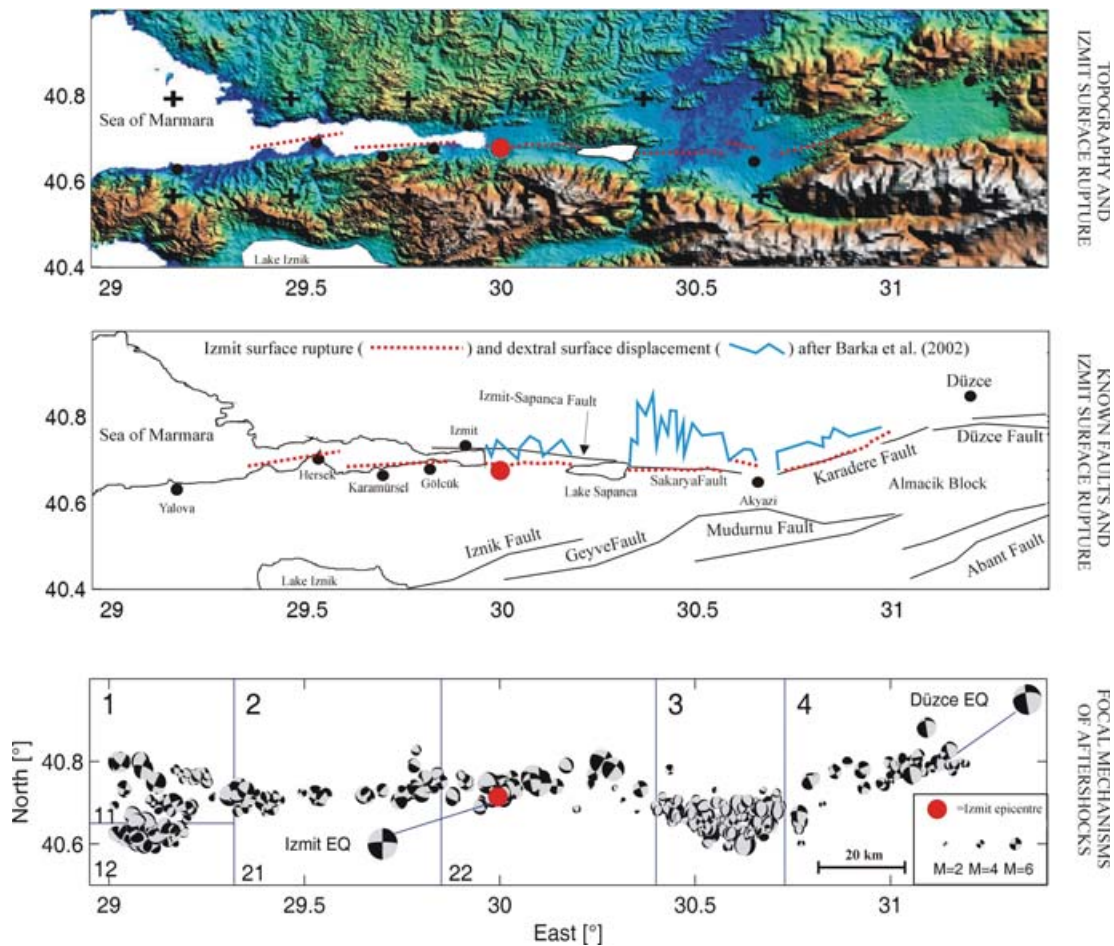
Figure 8. *Upper part:* Topographic map of the Izmit segment of the North Anatolian fault zone (after Fielding *et al.* 1999). Red dotted lines indicate the simplified surface rupture of the Izmit event (after Barka *et al.* 2002). The bold red dot indicates the epicentre of the Izmit mainshock. *Middle part:* Main faults of the NAFZ along the Izmit rupture area. Blue lines along the three onshore segments represent lateral distribution of surface slip after Barka *et al.* (2002) scaled to the slip maximum of ∼6 m. *Lower part:* Distribution of the 446 focal mechanisms analysed in this study (see also Fig. 2) and segmentation identified based on special clustering of focal mechanisms.

and Karadere-Düzce areas (our segments 2 and 4), aftershock focal mechanisms reflect mainly strike-slip and normal faulting. In general, the epicentres of individual events form trails delineating fault segments that correspond to one set of aftershock nodal planes (Fig. 2 and Fig. 8). E–W extensional normal faulting typifying the Akyazi plain of segment 3 (Fig. 5) is consistent with local topography at 30.6°E, which exhibits >500 m subsidence with respect to the surrounding area (Fig. 8). We interpret this plain to represent a small pull-apart basin similar to Lake Sapanca, Izmit Bay and the somewhat larger Sea of Marmara. In the following we relate aftershock segmentation along the rupture zone to the spatial distribution and temporal evolution of coseismic slip of the Izmit earthquake.

5.1.1 Coseismic slip along the Izmit rupture trace

Along the Izmit rupture, seismic moment release and coseismic slip vary from $>12*10^{19}$ N m and >5 m in high-slip zones to $<1*10^{19}$ N m and <1 m at low-slip barriers, respectively (e.g. Bouchon *et al.* 2002; Papageorgiou 2003). Mapped surface ruptures indicate five separate fault segments reaching from west to east separated by releasing (pull-apart) step-overs of about 1–4 km width (Tibi *et al.* 2001; Barka *et al.* 2002; Langridge *et al.* 2002; Polat *et al.* 2002,

see Fig. 8). From west to east, the segments are the Yalova-Hersek (striking N80°E), Karamürsel-Gölcük (N70°–80°E), Izmit-Sapanca (∼N90°E), Sapanca-Akyazi (N75°–85°E) and Karadere (N65°E). Step-overs between segments exhibit vertical offsets of up to 2.4 m, indicating a significant component of normal faulting that is in agreement with aftershock fault mechanisms at several locations along the rupture trace.

Coseismic rupture started at the main shock epicentre just west of Gölcük and propagated westwards along the Karamürsel-Gölcük segment with little moment release (Bos *et al.* 2004). Eastward propagation was triggered on the Izmit-Sapanca segment with a short delay resulting in asymmetric rupture of the main source (Delouis *et al.* 2002; Li *et al.* 2002). Rupture propagation was complex, involving several subevents possibly triggered on different fault segments. Total source duration, the number of subevents and the distribution of moment release after the first ∼20 s remain controversial (Tibi *et al.* 2001; Delouis *et al.* 2002; Gülen *et al.* 2002; Li *et al.* 2002; Bos *et al.* 2004). Using source-time functions of up to 90 s, 3–6 subevents have been identified (Tibi *et al.* 2001; Gülen *et al.* 2002).

Inversions of teleseismic, ground motion and space geodetic data also indicate distributed slip on separate fault segments with two slip maxima of 5–6 m near Gölcük and Lake Sapanca (e.g. Reilinger *et al.* 2000; Bouchon *et al.* 2002; Gülen *et al.* 2002; Li *et al.* 2002).

Table 2. Energy release, rupture area and average slip for the Izmit and Düzce mainshocks (coseismic) and the Izmit post-seismic time (after Bouchon *et al.* 2002; Bürgmann *et al.* 2002; Ergintav *et al.* 2002; Örgülü. & Aktar 2001; Reilinger *et al.* 2000; Tibi *et al.* 2001; Umutlu *et al.* 2004). See text for details.

	M_w	M_o $[10^{20} \text{ N m}]$	Rupture area $[\text{km}^2]$	Average slip $[\text{m}]$
Izmit mainshock	7.4	1.4–2.0	140×20	2.5–2.9
Düzce mainshock	7.1	0.5	60×20	0.8–1.0
Cumulative geodetic moment (Izmit-Düzce interevent time)	7.0	0.3	140×20	0.43
Izmit-Aftershocks (30 largest)	6.6	0.012	140×20	0.017
Izmit-Aftershocks (4400 largest)	6.8	0.025	140×20	0.036

Slip maxima were found between the surface and about 12 km depth. Delouis *et al.* (2002) presented a joint inversion of InSAR, GPS, teleseismic and strong motion data (see also Salichon *et al.* 2003) delineating four fault segments. Maximum slip is up to 8 m at about 6–12 km depth below Gölcük-Izmit and Lake Sapanca. The Akyazi plain (30.4–30.7°E) is consistently identified as an area of reduced slip (<1 m).

5.1.2 Aftershock activity and post-seismic slip along the Izmit rupture trace

Post-seismic slip estimated from GPS over the 75 days following the Izmit earthquake was about 0.43 m. The corresponding total geodetic moment is equivalent to $M_w = 7.0$ (Reilinger *et al.* 2000; Bürgmann *et al.* 2002; Ergintav *et al.* 2002) and, therefore, one order of magnitude higher than the moment liberated by the 4000 largest aftershocks (see Table 2). This indicates that post-seismic deformation was largely aseismic. Modelling of afterslip suggests that maximum creep is expected at depths of >20 km (Reilinger *et al.* 2000).

The maxima of coseismic and post-seismic slip and the aftershock activity are anti-correlated. For example, the minima of aftershock activity in the Hersek Delta (29.6°E) and in the Lake Sapanca (30.2°E–30.3°E) in segment 2 (Fig. 4) and near Karadere (30.8°E) in segment 4 (Fig. 6) coincide with the corresponding coseismic slip maxima. High coseismic slip in the Izmit-Sapanca (segment 2) and Karadere-Düzce (segment 4) areas is correlated with a predominantly strike-slip faulting regime of the aftershocks. In contrast, high rates of aftershock activity and abundant normal faulting events in the Akyazi area and at the western end of the rupture trace coincide with low slip at barriers and step-overs between fault segments.

Significant afterslip occurred at depth along the eastern Karadere segment close to the epicentre of the Düzce mainshock ($M_w = 7.1$, 1999 November 12). Interestingly, we observe a relatively high rate of aftershock activity in this region. Focal mechanisms of the three largest aftershocks on this segment (M ≥ 4, Fig. 6) are very similar to Izmit subevent S2 and the Düzce event (both indicated in Fig. 1), which occurred 30 s and about three months after the Izmit earthquake, respectively. The three aftershock events all occurred within 6 hours after the Izmit mainshock. In contrast, fault plane solutions of small aftershocks show a larger variability, which was not observed on any of the three segments to the west. This observation suggests that small events also reflect small-scale structural complexity of the NAFZ. With increasing magnitude, focal mechanisms

increasingly reveal the orientation of the regional stress field orientation. This effect has also been observed for fluid-injection induced microseismicity (Bohnhoff *et al.* 2004), but at a lower magnitude level ($-1 < M_w < 1$).

5.2 Evolution of the stress field at the NAFZ

To analyse spatial and temporal variations of the stress field along the NAFZ and especially along the Izmit rupture we collected all available information on the long-term regional stress field in NW Turkey covering the past ∼5 decades. In addition, we performed stress tensor inversion of focal mechanisms of events prior ('pre-seismic') and during ('coseismic') the Izmit mainshock. The entire set of information on stress field orientation in the area of investigation is summarized in Table 1. Information on the long-term regional stress field in NW Turkey was taken from the World Stress Map data base (Heidbach *et al.* 2004; Reinecker *et al.* 2004) which contains 13 stress orientation measurements for the area of interest indicating a mean maximum horizontal stress (S_H) trending N124°E. In addition, Kiratzi (2002) performed stress tensor inversion of the 11 largest earthquakes that had occurred in the region since 1943 and revealed a strike-slip faulting regime with subhorizontal NW–SE-trending orientation of the maximum principal stress and a near-vertical intermediate principal stress. Further information on the pre-seismic stress field was obtained from inverting focal mechanisms obtained with a local network in the easternmost Sea of Marmara during 1996 January–September (Ergin *et al.* 1997).

The 'coseismic' stress field during the Izmit event was determined by inverting the focal mechanisms of the six Izmit subevents constituting the entire Izmit rupture (Gülen *et al.* 2002). Furthermore, the 30 largest aftershocks (Örgülü & Aktar 2001) were used to derive the regional 'post-seismic' stress field. Interestingly, this data set contains only three EW-extensional normal faulting events within the Akyazi Plain and yields a well-defined stress regime almost identical to the 'pre-seismic' regional stress field (Table 1).

In Fig. 9 the stress field orientations of the data sets as described above are shown in chronological order. The angle between the trend of σ_1 and the regional trend of the NAFZ (N90°E) is indicated by the black lines and the grey-shaded areas represent their standard deviation. The stress field orientations of Kiratzi (2002) and from the World Stress Map are identical to within ≤2°. We consider this orientation to represent the long-term regional stress field in NW Turkey. Notably, the regional stress field orientation is almost identical with the local stress field orientation during the Izmit earthquake with both confidence regions in the range of 12°. The local stress field within the eastern Sea of Marmara in 1996 differs by ∼10° with the regional stress field while the 68 per cent confidence regions overlap.

The stress field after the Izmit mainshock is spatially heterogeneous along the rupture. Orientations of the principal stresses vary significantly between segments 1–4 reflecting fault complexity. For segments 1, 2 and 4 the maximum compressive stress direction σ_1 is subhorizontal and trends N117°E to N159°E. We, therefore, approximate its azimuth by the azimuth of the largest near-horizontal stress (SH) and thus equate σ_1 with SH in segments 1,2 and 4 (in segment 3, σ_1 is almost vertical, see Fig. 7, Table 1). Note, that the accuracy for the orientations of σ_{1-3} is in the range of 6–8° for one standard deviation (68 per cent) and, therefore, unprecedently small for this region. We interpret the strong partitioning of the post-seismic stress field to reflect the local fault structure along the rupture. A striking result of the stress inversion of the aftershock focal mechanisms
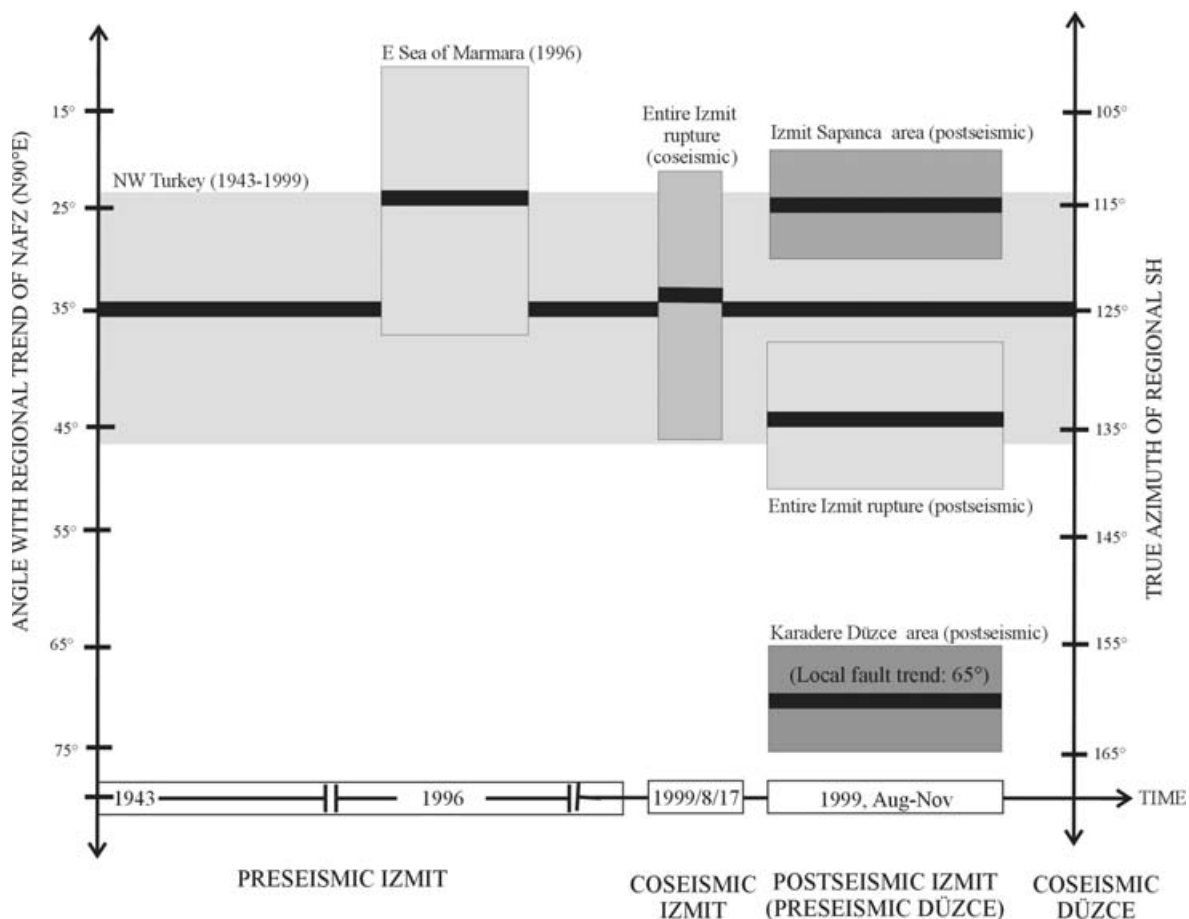
Figure 9. Evolution of stress field orientation in NW Turkey along the Izmit rupture. The diagram displays the angle between the trend of the maximum compressional stress (σ_1) and the regional trend of the NAFZ (N90°E) plotted versus time for the different data sets considered in this study (see Table 1 for details). The horizontal extension of the rectangles marks the time interval covered by their data content. Black line marks the best resolved orientation whereas grey intervals represent the confidence region (68 per cent).

in the Izmit-Sapanca (segment 2) and Karadere-Düzce (segment 4) areas is that the local stresses are rotated compared to the regional stress field and local fault trend. A change of the state of stress in the vicinity of coseismic slip maxima may have reactivated secondary faults and modified the local fault structure. In particular, shear failure and the associated drop in shear stress may result in a rotation of the principal stresses acting on the fault. This has been observed for some earthquakes at strike-slip and reverse faults in California such as the 1983 Coalinga (Michael 1987b), 1986 Oceanside (Hauksson & Jones 1988), 1989 Loma Prieta (Michael *et al.* 1990; Zoback & Beroza 1993), 1992 Landers (Hauksson 1994; Hardebeck & Hauksson 1999, 2001), and 1994 Northridge (Zhao *et al.* 1997) earthquakes. Stress ratios varied notably indicating local transtensional faulting ($R = 0.43–0.65$, Hauksson 1994) and transpression ($R = 0.2–0.55$, Michael *et al.* 1990). Principal stresses were horizontally rotated significantly between about 10°–20° in a clockwise and counter-clockwise direction. In some cases (Northridge, Coalinga, Landers) stress rotations reversed with time and varied along the rupture trace. Notwithstanding that stress rotations during the seismic cycle and especially in connection with large earthquakes are in accordance with the present understanding of faulting kinematics, observed stress rotations should be interpreted with care as was shown for the case of Landers by Townend & Zoback (2001).

Local rotations of the stress field at a fault are extremely difficult to detect. The accuracy of stress field determination is limited

to ~5° at best, which is mainly due to the uncertainty in orientation of focal mechanisms used for the stress inversion. Often, these errors in stress field orientation are of the same order of or only slightly less than the magnitude of the expected rotations. In the Izmit-Sapanca area (segment 2) we observe a counter-clockwise rotation of the post-seismic stress field with respect to the long-term regional and coseismic stress field of about 8°. In this part of the NAFZ a more or less uniform EW-trending fault was activated during the Izmit mainshock. Interestingly, the hypocentral distribution of aftershocks in this area shows the same ~10° counter-clockwise rotation with respect to the local coseismic fault trend (Fig. 10) indicating that the mainshock stress drop induced a local rotation of the stress field that resulted in activation of optimally oriented secondary faults. Stress rotation is also observed at the eastern termination of the Izmit rupture (Karadere-Düzce area, segment 4). Here, the local fault trend of the NAFZ is N65°E along the Karadere segment where most of the Izmit aftershocks in segment 4 occurred. The post-seismic orientations of the three principal stresses in this area are well resolved (see Fig. 7). With respect to the regional stress field we identify a 34° clockwise rotation of the local stress field along the Karadere segment due to the mainshock. As in the Izmit-Sapanca area, the rotation of the local stresses is consistent with the local trend formed by the distribution of hypocentres that indicate a rotation of ~25° (Fig. 10). However, at the Karadere segment the stress rotation occurred in a clockwise direction
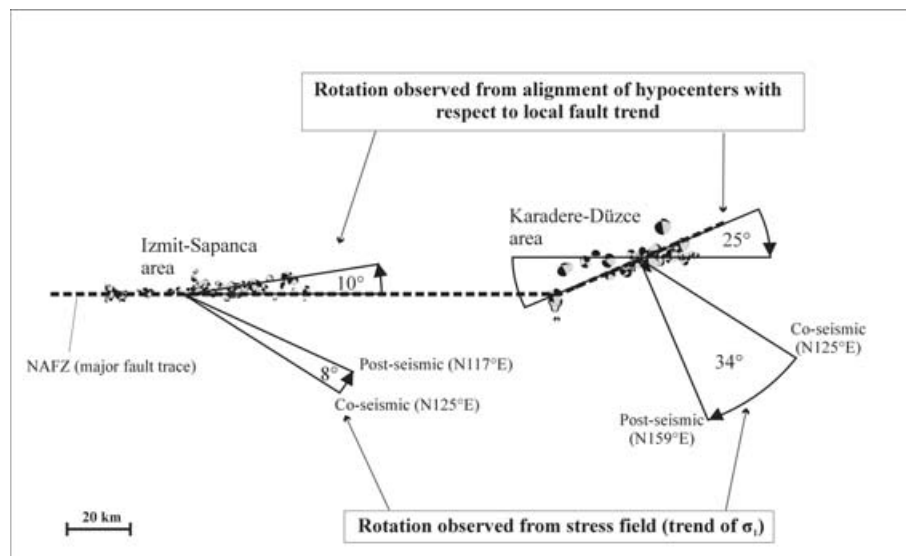
Figure 10. Rotation of the local stress field orientation in the Izmit-Sapanca and Karadere-Düzce areas. Plotted is the coseismic and the post-seismic trend of σ_1 for either area. The bold arrows document the observed rotations in counter-clockwise and clockwise direction in the Izmit-Sapanca and Karadere-Düzce areas, respectively. In addition we plotted the hypocentral distribution of aftershock focal mechanisms for either area. Relating the trend of their alignment to the local fault trend we observe a similar rotation as for σ_1 indicating that the Izmit mainshock caused stress rotation that result in activation of secondary faults.

compared to the Izmit Sapanca segment, where the observed rotation was counter-clockwise. We suggest that the different sense of rotation of the post-seismic stress field is related to the varying trends of the NAFZ segments in relation to the regional stress field producing different loading states along the fault trace. In the central region around the Izmit epicentre, stress drop associated with the Izmit main event reduced the shear stresses acting on the fault segment causing stresses to rotate counter-clockwise. However, stress release at the eastern part of the rupture seems to have produced a progressive clockwise rotation of the static stress field, since the Karadere segment is exposed differently to the regional principal stresses by about 25°. The $M_w = 7.1$ Düzce mainshock extended the Izmit rupture into a region of positive Coulomb stress (e.g. Parsons *et al.* 2000). However, it was also affected by an increasingly rotated stress field as shown in this study.

6 CONCLUSIONS

We have investigated aftershock focal mechanisms of the $M_w = 7.4$ Izmit earthquake of 1999 August 17, on the western NAFZ. Aftershock clusters define 4 individual fault segments. Focal mechanisms surrounding epicentres of the Izmit and subsequent Düzce mainshock ($M_w = 7.1$, 12.11.99) indicate dominantly strike-slip but also normal faulting. Aftershocks in the area between Izmit and Düzce segments are mainly related to EW-extensional normal faulting indicating a small pull-apart structure. West of the Izmit mainshock, alignments of aftershocks suggest branching of the North Anatolian fault into three or more active segments differing significantly in dominant focal mechanisms. Areas with high coseismic slip show aftershocks that are dominantly strike-slip, but low-slip barriers show mostly normal faulting aftershocks.

Stress tensor inversions of the focal mechanisms show a clear stress partitioning and rotations of the local stress field following the Izmit mainshock. In the Izmit-Sapanca area the direction of the maximum compressive stress is rotated counter-clockwise with respect to the regional stress field. Towards the eastern end of

the rupture (Karadere-Düzce area) stresses are rotated clockwise. In both areas the stress rotation is consistent with the alignment of aftershock hypocentres. We suggest that the opposing rotations of the post-seismic stress field is related to the locally varying trend of the NAFZ segments in relation to the regional stress field that results in different loading states along the fault trace through time. The observed temporal variations in orientation of the principal stresses are significant, but can only be detected by dense local networks with a low magnitude threshold permitting the determination of highly confident focal mechanisms as the basis for stress inversion. We expect that the observed spatiotemporal changes of the stress field should affect the modelling of optimally oriented faults from Coulomb failure stress analysis and thus local estimates of seismic hazard.

REFERENCES

Armijo, R., Meyer, B., Hubert, A. & Barka, A., 1999. Westward propagation of the North Anatolian Fault into the northern Aegean: timing and kinematics, *Geology,* **27**, 267–270.

Barka, A. *et al.*, 2002. The Surface Rupture and Slip Distribution of the 17 August 1999 Izmit Earthquake (M 7.4), North Anatolian Fault, *Bull. seism. Soc. Am.,* **92**(1), 43–60.

Baris, S., Ito, A., Ücer, S.B., Honkura, Y., Kafadar, N., Pektas, R., Komut, T. & Isikara, A.M., 2002. Microearthquake activity before the

Izmit earthquake in the Eastern Marmara Region, Turkey (1 January 1993–17 August 1999), *Bull. seism. Soc. Am.,* **92**(1), 394–405.

Baumbach, M. *et al.*, 2003. Calibration of an Ml Scale in Northwestern Turkey from 1999 Izmit aftershocks, *Bull. seism. Soc. Am.,* **93**(5), 2289–2295.

Bohnhoff, M., Baisch, S. & Harjes, H.-P., 2004. Fault mechanisms of induced seismicity at the superdeep German Continental Deep Drilling Program (KTB) borehole and their relation to fault structure and stress field, *J. geophys. Res.,* **109**, B02309, doi:10.1029/2003JB002528.

Bos, A.G., Usai, S. & Spakman, W., 2004. A joint analysis of GPS motions and InSAR to infer the coseismic surface deformation of the Izmit, Turkey earthquake, *Geophys. J. Int.,* **158**, 849–863.

Bouchon, M., Töksöz, M.N., Karabulut, H., Bouin, M.-P., Dietrich, M., Aktar, M. & Edie, M., 2002. Space and Time Evolution of Rupture and Faulting during the 1999 Izmit (Turkey) Earthquake, *Bull. seism. Soc. Am.,* **92**(1), 256–266.

Bürgmann, R., Ergintav, S., Segall, P., Hearn, E.H., McClusky, S., Reilinger, R.E., Woith, H. & Zschau, J., 2002. Time-dependent Distributed Afterslip on and Deep below the Izmit Earthquake Rupture, *Bull. seism. Soc. Am.,* **92**(1), 126–137.

Delouis, B., Giardini, C., Lundgren, P. & Salichon, J., 2002. Joint inversion of InSAR, GPS, Teleseismic, and Strong-Motion Data for the Spatial and Temporal Distribution of Earthquake slip: Application to the 1999 Izmit Mainshock, *Bull. seism. Soc. Am.,* **92**(1), 278–299.

Ergin, M., Aktar, M., Bicmen, F., Yörük, A., Namik Yalcin, M. & Kuleli, S., 1997. Detailed microearthquake monitoring of the Izmit Bay, Aktif Tektonik Arastirma Grubu Birinci Toplantisi, ITÜ Istanbul (in Turkish).

Ergintav, S., Bürgmann, R., McClusky, S., Cakmak, R., Reilinger, R.E., Lenk, O., Barka, A. & Özener, H., 2002. Postseismic Deformation near the Izmit Earthquake (17 August 1999, M 7.5) Rupture Zone, *Bull. seism. Soc. Am.,* **92**(1), 194–207.

Fielding, E.J., Wright, T.J., Parsons, B.E., England, P.C., Rosen, P.A., Hensley, S. & Bilham, R., 1999. Topography of northwest Turkey from SAR interferometry: applications to the 1999 Izmit earthquake geomorphology and coseismic strain, *EoS Trans. Am. geophys. Un.,* **80**, 46, F762.

Flerit, F., Armijo, R., King, G. & Meyer, B., 2004. The mechanical interaction between the propagating North Anatolian Fault and the back-arc extension in the Aegean, *EPSL,* **224**, 347–362.

Gephart, J.W., 1990. Stress and the direction of slip on fault planes, *Tectonics,* **9**, 845–858.

Gephart, J.W. & Forsyth, D.W., 1984. An improved Method for Determining the Regional Stress Tensor Using Earthquake Focal Mechanism Data: Application to the San Fernando Earthquake Sequence, *J. geophys. Res.,* **89**, 9305–9320.

Grosser, H. *et al.*, 1998. The Erzincan (Turkey) Earthquake (M_s 6.8) of March 13, 1992 and its aftershock sequence, *Pageoph,* **152**, 465–505.

Gülen, L., Pinar, A., Kalafat, D., Özel, N., Horasan, G., Yilmazer, M. & Isikara, A.M., 2002. Surface breaks. Aftershock Distribution, and Rupture Process of the 17 August 1999 Yzmit, Turkey, Earthquake, *Bull. seism. Soc. Am.,* **92**(1), 230–244.

Gurbuz, C. *et al.*, 2000. The seismotectonics of the Marmara region (Turkey): results from a microseismic experiment, *Tectonophysics,* **316**, 1–17.

Hardebeck, J.L. & Hauksson, E., 1999. Role of fluids in faulting inferred from stress field signatures, *Science,* **285**, 236–239.

Hardebeck, J.L. & Hauksson, E., 2001. Crustal stress field in southern California and its implications for fault mechanics, *J. geophys. Res.,* **106**, 21 859–21 882.

Hauksson, E., 1994. State of stress from focal mechanisms before and after the 1992 Landers earthquake sequence, *Bull. seism. Soc. Am.,* **84**, 917–934.

Hauksson, E. & Jones, L.M., 1988. The July 1986 Oceanside ($M_l = 5.3$) earthquake sequence in the continental borderland, southern California, *Bull. seism. Soc. Am.,* **78**(6), 1885–1906.

Heidbach, O. *et al.*, 2004. Stress maps in a minute: the 2004 World Stress Map release, *EOS, Trans. Am. geophys. Un.,* **85**(49), 521–529.

Karabulut, H., Bouin, M.P., Bouchon, M., Dietrich, M., Cornou, C. & Aktar, M., 2002. The seismicity in the Eastern Marmara Sea after the 17 August 1999 Yzmit earthquake, *Bull. seism. Soc. Am.,* **92**(2), 387–393.

Kiratzi, A., 2002. Stress tensor inversions along the westernmost North Anatolian fault zone and its continuation into the North Aegean Sea, *Geophys. J. Int.,* **151**, 360–376.

Kiratzi, A. & Louvari, E., 2001. Source parameters of the Izmit-Bolu 1999 (Turkey) earthquake sequences from teleseismic data, *Ann. Geophysics,* **44**, 33–47.

Langridge, R.M., Stenner, H.D., Fumal, T.E., Christofferson, S.A., Rockwell, T.K., Hartleb, R.D., Bachhuber, J. & Barka, A.A., 2002. Geometry, slip distribution, and kinematics of surface rupture on the Sakarya fault segment during the 17 August 1999 Yzmit, Turkey, earthquake, *Bull. seism. Soc. Am.,* **92**(1), 107–125.

Li, X., Cormier, V.F. & Töksöz, M.N., 2002. Complex Source Process of the 17 Aug 1999 Yzmit, Turkey, earthquake, *Bull. seism. Soc. Am.,* **92**(1), 267–277.

McClusky, S. *et al.*, 2000. Global positioning system constraints on plate kinematics and dynamics in the eastern Mediterranean and Caucasus, *J. geophys. Res.,* **105**, 5695–5719.

Michael, A.J., 1984. Determination of stress from slip data; faults and folds, *J. geophys. Res.,* **89**, 11 517–11 526.

Michael, A.J., 1987a. Use of focal mechanisms to determine stress: a control study, *J. geophys. Res.,* **92**, 357–368.

Michael, A., 1987b. Stress rotation During the Coalinga Aftershock Sequence, *J. geophys. Res.,* **92**, 7963–7979.

Michael, A.J., 1991. Spatial variations in stress within the 1987 Whittier Narrows, California, aftershock sequence: new techniques and results, *J. geophys. Res.,* **96**, 6303–6319.

Michael, A.J., Ellsworth, W.L. & Oppenheimer, D.H., 1990. Coseismic stress changes induced by the 1989 Loma Prieta, California earthquake, *Geophys. Res. Lett.,* **17**(9), 1441–1444.

Milkereit, C. *et al.*, 2000. Preliminary aftershock analysis of $M_w = 7.4$ Izmit and $M_w = 7.1$ Düzce earthquake in Western Turkey. In: Barka, A., Ö. Kozaci, S. Akyüz (Editors): The 1999 Izmit and Düzce Earthquakes: preliminary results. pp. 179–187, Istanbul Technical University.

Noomen, R., Springer, T.A., Ambrosius, B.A.C., Herzberger, K., Kuijper, D.C., Mets, G.-J., Overgaauw, B. & Wakker, K.F., 1996. Crustal deformations in the Mediterranean Area computed from SLR and GPS observations. *J. Geodyn.,* **21**(1), 73–96.

Örgülü, G. & Aktar, M., 2001. Regional moment tensor inversion for strong aftershocks of the August 17, 1999 Izmit earthquake ($M_w = 7.4$), *Geophys. Res. Lett.,* **28**(2), 371–374.

Özalaybey, S., Ergin, M., Aktar, M., Tapirdamaz, C., Bicman, F. & Yörük, A., 2002. The 1999 Izmit earthquake sequence in Turkey: seismological and tectonic aspects, *Bull. seism. Soc. Am.,* **92**(2), 376–386.

Papageorgiou, A.S., 2003. The barrier model and strong ground motion, *Pageoph,* **160**, 603–634.

Parsons, T., 2004. Recalculated probability of $M \geq 7$ earthquakes beneath the Sea of Marmara, Turkey, *J. geophys. Res.,* **109**, doi:10.1029/2003JB002667.

Parsons, T., Toda, S., Stein, R.S., Barka, A. & Dieterich, J.H., 2000. Heightened odds of large earthquakes near Istanbul: an interaction-based probability calculation, *Science,* **288**, 661–664.

Polat, O., Eyidogan, H., Haessler, H., Cisternas, A. & Philip, H., 2002. Analysis and interpretation of the aftershock sequence of the August 17, 1999, Izmit (Turkey) earthquake, *J. Seismol.,* **6**, 287–306.

Reasenberg, P.A. & Oppenheimer, D., 1985. FPFIT, FPPLOT, and FPPAGE: Fortran computer programs for calculating and displaying earthquake fault plane solutions. Dept. of Interior, *US Geological Survey, Open-file report,* **85–739**, 109pp.

Reilinger, R.E. *et al.*, 2000. Coseisic and postseismic fault slip for the 17 August 1999, *M* = 7.5, Izmit, Turkey earthquake, *Science,* **289**, 1519–1524.

Reinecker, J., Heidbach, O., Tingay, M., Connolly, P. & Müller, B., 2004. The 2004 release of the World Stress Map (available online at www.world-stress-map.org).

Salichon, J., Delouis, B., Lundgren, P., Giardini, D., Constantini, M. & Rosen, P., 2003. Joint inversion of broadband teleseismic and interferometric synthetic aperture radar (InSAR) data for the slip history of the

M_{w} = 7.7, Nazca ridge (Peru) earthquake of 12 November 1996, *J. geophys. Res.,* **108**, 2085, doi:10.1029/2001JB000913.

Stein, R., 1999. The role of stress transfer in earthquake occurrence, *Nature,* **402**, 605–609.

Stein, R.S., Barka, A. & Dieterich, J.H., 1997. Progressive failure ob the North Anatolian fault since 1939 by earthquake stress triggering, *Geophys. J. Int.,* **128**, 594–604.

Tibi, R. *et al.*, 2001. Rupture processes of the 1999 August 17 Izmit and November 12 Düzce (Turkey) earthquakes, *Geophys. J. Int.,* **144**, F1–F7.

Töksöz, M.N., Shakal, A.F. & Michael, A.J., 1979. Space-time migration of earthquakes along the North Anatolian Fault and seismic gaps, *Pageoph,* **117**, 1258–1270.

Townend, J. & Zoback, M.D., 2001. Implications of earthquake focal mech-
anisms for the frictional strength of the San Andreas fault system, *Geol. Soc. Spec. Publ.,* **186**, 13–21.

Umutlu, N., Koketsu, K. & Milkereit, C., 2004. The rupture process during the 1999 Düzce, Turkey, earthquake from joint inversion of teleseismic and strong-motion data, *Tectonophysics,* **391**, 315–324.

Wright, T., Fielding, E. & Parsons, B., 2001. Triggered slip: observations of the 17 August 1999 Izmit (Turkey) earthquake using radar interferometry, *Geophys. Res. Lett.,* **28**(6), 1079–1082.

Zhao, D., Kanamori, H. & Wiens, D., 1997. State of stress before and after the 1994 Northridge earthquake, *Geophys. Res. Lett.,* **24**(5), 519–522.

Zoback, M.D. & Beroza, G.C., 1993. Evidence for near-frictionless faulting in the 1989 (M 6.9) Loma Prieta, California, earthquake and its after-shocks. *Geology,* **21**(2), 181–185.